Title
Isosinglet down quark mixing and CP violation experiments

Journal
Physical Review D, 66(1)

ISSN
2470-0010

Authors
Hawkins, Donovan
Silverman, Dennis

Publication Date
2002-07-01

DOI
10.1103/physrevd.66.016008

Isosinglet down quark mixing and CP violation experiments

Donovan Hawkins and Dennis Silverman*
Department of Physics and Astronomy, University of California, Irvine, Irvine, California 92697-4575
(Received 1 May 2002; published 31 July 2002)

We confront the new physics models with extra isosinglet down quarks in the new CP violation experimental era with $\sin(2\beta)$ and ϵ'/ϵ measurements, $K^+\to\pi^+\nu\bar{\nu}$ events, and x_s limits. The closeness of the new experimental results to the standard model theory requires us to include full standard model (SM) amplitudes in the analysis. In models allowing mixing to a new isosinglet down quark, as in E_6, flavor changing neutral currents are induced that allow a Z^0 mediated contribution to B-$\bar{B}$ mixing and which bring in new phases. In (ρ,η), $(x_s,\sin(\gamma))$, and $(x_s,\sin(2\phi_s))$ plots we still find much larger regions in the four down quark model than in the SM, reaching down to $\eta\approx 0$, $0\leqslant\sin(\gamma)\leqslant 1$, $-0.75\leqslant\sin(2\alpha)\leqslant 0.15$, and $\sin(2\phi_s)$ down to zero, all at 1σ. We elucidate the nature of the cancellation in an order λ^5 four down quark mixing matrix element which satisfies the experiments and reduces the number of independent angles and phases. We also evaluate tests of unitarity for the 3×3 Cabibbo-Kobayashi-Maskawa submatrix.

DOI: 10.1103/PhysRevD.66.016008 PACS number(s): 11.30.Er, 12.15.Hh, 12.15.Mm, 12.60.−i

I. INTRODUCTION

The "new physics" class of models we use are those with extra isosinglet down quarks, where we take only one new down quark as mixing significantly. An example is E_6, where there are two down quarks for each generation with only one up quark, and of which we assume only one new isosinglet down quark mixes strongly. This model has shown large possible effects in B-$\bar{B}$ mixing phases [1]. The new B factory results on $\sin(2\beta)$ in the standard model (SM) range, the ϵ'/ϵ experimental convergence, the new $K^+\to\pi^+\nu\bar{\nu}$ result, the Δm_s limits near the SM prediction, and other new measurements require a finer analysis and a potential challenge to new physics models. In this paper we include the full SM contributions as well as the new physics contributions from the isosinglet down quark model to jointly analyze the constraints from all of these experiments, as well as other flavor changing neutral current (FCNC) limits and SM Cabibbo-Kobayashi-Maskawa (CKM) matrix element constraints.

In models allowing mixing to a new isosinglet down quark (as in E_6) flavor changing neutral currents are induced that allow a Z^0 mediated contribution to B-$\bar{B}$ mixing and which bring in new phases [1–3]. In (ρ,η), $(x_s,\sin(\gamma))$, and $(x_s,\sin(2\phi_s))$ plots we still find much larger regions than in the SM, reaching down to $\eta\approx 0$, $0\leqslant\sin(\gamma)\leqslant 1$, and $\sin(2\phi_s)$ down to zero (below the SM range), all at 1σ limits. The nature of the cancellation in a fourth down quark matrix element V_{4d} to satisfy the experiments is elucidated. We also establish ranges for the new mixing elements to the new isosinglet down quark, and make a simple estimate of the lower mass limit of the new down quark.

In Sec. II we introduce the scenario with more down quarks as in E_6, truncate it to one extra down quark, introduce the 4×4 mixing matrix, and apply it to B-$\bar{B}$ mixing. Section III presents the CP violating B_d and B_s decay asymmetries, and B_s mixing, including the FCNC tree diagram additions. Section IV presents the full SM contributions as well as the four down quark model (FDQM) amplitudes for the CP violating and FCNC K meson experiments that are used. Section V presents the joint chi-squared analysis and results for the SM and FDQM model for the various plots listed above. Section VI presents the sizes or limits on the matrix elements, mixing angles, phases, FCNC couplings and unitarity quadrangles. Section VII lists the conclusions and projects what the next down quark mass limit might be.

II. ISOSINGLET DOWN QUARK MIXING MODEL

Groups such as E_6 with extra $SU(2)_L$ singlet down quarks [4] give rise to flavor changing neutral currents (FCNC) through the mixing of four or more down quarks [3,5–8]. The initial quarks of definite weak isospin in E_6, for each generation are the left handed isodoublet (u^0_{iL},d^0_{iL}), their right handed isosinglets u^0_{iR} and d^0_{iR}, and the yet to be found isosinglet pairs D^0_{iL} and D^0_{iR}.

We can take the initial up quark matrix to be the mass eigenstates, so $u^0_i=u_i$, giving $V^u=I_{3\times 3}$. The down quarks (d^0_i,D^0_i), which correspond to the same generations as u_i, mix to form mass eigenstates (d_i,D_i) via the matrix $V^d(6\times 6)$, where $d^0_{iL}=V^d_{ij}d_{jL}$. The weak interaction charged current matrix is then $U=V^{u\dagger}\times V^d$, the 3×6 matrix that is the upper three rows of V^d. The lower three rows of V^d are the three linear combinations of (d_i,D_i) that are the isosinglet D^0_i which cannot couple to up quarks by the weak interactions.

We truncate the V^d matrix to the 4×4 matrix using only the D quark that mixes most (and dropping the superscript d on V^d), giving the four down quark model (FDQM). Calling the new down quark mixture D, the weak charged currents of D to u, c, and t quarks are $V_{tD}=s_{34}$, $V_{cD}=s_{24}e^{-i\delta_{24}}$, and $V_{uD}=s_{14}e^{-i\delta_{14}}$, which are in the fourth column. The fourth row gives the linear combination that is the initial isosinglet D^0_L. The complete 4×4 mixing matrix was given previously [9,10]. The leading terms in the 4×4 down quark mixing matrix with 6 angles and 3 phases are

*Email address: djsilver@uci.edu

$$V=\begin{array}{c} \\ u\\ c\\ t\\ 4\end{array}\left(\begin{array}{cccc} d & s & b & D\\ c_{12}c_{34} & s_{12}c_{34} & s_{13}e^{-i\delta_{13}} & s_{14}e^{-i\delta_{14}}\\ -s_{12} & 1 & s_{23} & s_{24}e^{-i\delta_{24}}\\ (s_{12}s_{23}-s_{13}e^{i\delta_{13}}) & -s_{23} & 1 & s_{34}\\ V_{4d} & V_{4s} & V_{4b} & V_{44}\end{array}\right), \tag{1}$$

where, to leading order in new angles,

$$V^*_{4d}=-s_{14}e^{-i\delta_{14}}+s_{24}e^{-i\delta_{24}}s_{12}-s_{34}(s_{12}s_{23}-s_{13}e^{-i\delta_{13}}), \tag{2}$$

$$V^*_{4s}=-s_{24}e^{-i\delta_{24}}-s_{14}e^{-i\delta_{14}}s_{12}+s_{34}(s_{23}+s_{12}s_{13}e^{-i\delta_{13}}), \tag{3}$$

$$V^*_{4b}=-s_{34}-s_{24}e^{-i\delta_{24}}s_{23}-s_{14}e^{-i\delta_{14}}s_{13}e^{i\delta_{13}}. \tag{4}$$

A. FCNC in Z^0 couplings from extra isosinglet down quarks

The FCNC amplitudes are given in terms of the mixings V_{4i} to form the isosinglet down quark by [5]

$$-U_{ij}\equiv V^*_{4i}V_{4j} \quad \text{for} \quad i\neq j. \tag{5}$$

The FCNC couplings of the down quarks to the Z^0 are then given by

$$\mathcal{L}^Z_{FCNC}=-\frac{e}{2\sin\theta_W\cos\theta_W}U_{ij}\overline{d}_{iL}\gamma^\mu d_{jL}Z_\mu. \tag{6}$$

The flavor changing neutral currents are [7,8] $-U_{sd}=V^*_{4s}V_{4d}$, $-U_{sb}=V^*_{4s}V_{4b}$, and $-U_{bd}=V^*_{4b}V_{4d}$.

The diagonal neutral current couplings are reduced in strength by the amplitudes into the isosinglet down quarks, becoming

$$\mathcal{L}^Z_{NC}=-\frac{e}{2\sin\theta_W\cos\theta_W}\sum_i(1-|V_{4i}|^2)\overline{d}_{iL}\gamma^\mu d_{iL}Z_\mu. \tag{7}$$

The FCNC with tree level Z^0 mediated exchange may contribute part of B^0_d-$\overline{B}^0_d$ mixing and of B^0_s-$\overline{B}^0_s$ mixing, and the constraints leave a range of values for the fourth quark's mixing parameters. As shown in Fig. 1, B^0_d-$\overline{B}^0_d$ mixing may occur by the $\overline{b}$-d quarks in a B_d annihilating to a virtual Z through a FCNC with amplitude U_{bd}, and the virtual Z then creating b-$\overline{d}$ quarks through another FCNC, again with amplitude U_{bd}, which then becomes a $\overline{B}_d$ meson.

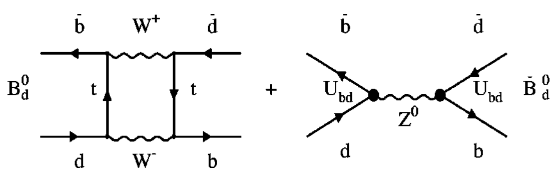

FIG. 1. The SM second order weak box diagram plus the double FCNC vertex tree diagram with an intermediate Z^0 for B_d-$\overline{B}_d$ mixing.

If the FCNC amplitudes are a large contributor to the B_d-$\overline{B}_d$ mixing, they introduce three new mixing angles and two new phases over the standard model (SM) into the CP violating B decay asymmetries. The size of the contribution of the FCNC amplitude U_{db} as one side of the unitarity quadrangle is less than 0. 15 of the unit base $|V_{cd}V_{cb}|$ at the 1-σ level (see Sec. VI), but we have found [3,5,7,8] that it can contribute as large an amount to B_d-$\overline{B}_d$ mixing as does the standard model. The new phases can appear in this mixing and give total phases different from that of the standard model in CP violating B decay asymmetries [7–9,11,12].

For B_d-$\overline{B}_d$ mixing with the four down quark induced b-d coupling, U_{db}, we have [9]

$$x_d=(2G_F/3\sqrt{2})B_Bf_B^2m_B\eta_B\tau_B|U^2_{std-db}+U^2_{db}|, \tag{8}$$

where with $y_t=m_t^2/m_W^2$,

$$U^2_{std-db}\equiv[\alpha/(4\pi\sin^2\theta_W)]y_tf_2(y_t)(V^*_{td}V_{tb})^2, \tag{9}$$

and $x_d=\Delta m_{B_d}/\Gamma_{B_d}=\tau_{B_d}\Delta m_{B_d}$. In order to compare magnitudes, in the SM, $U^2_{std-db}=0.50\times10^{-6}(1-\rho+i\eta)^2$.

The CP violating decay asymmetries depend on the combined phases of the B^0_d-$\overline{B}^0_d$ mixing and the b quark decay amplitudes into final states of definite CP. Since we have found that Z mediated FCNC processes may contribute significantly to B^0_d-$\overline{B}^0_d$ mixing, the phases of U_{db} would be important. The FCNC amplitude U_{db} to leading order in the new angles is

$$U_{db}=(-s_{34}-s_{24}s_{23}e^{i\delta_{24}})(s_{34}V^*_{td}+s_{14}e^{-i\delta_{14}}-s_{24}e^{-i\delta_{24}}s_{12}), \tag{10}$$

where $V_{td}\approx(s_{12}s_{23}-s_{13}e^{i\delta_{13}})$, and $V_{ub}=s_{13}e^{-i\delta_{13}}$.

III. MIXING AND CP VIOLATING DECAY ASYMMETRIES IN THE FOUR DOWN QUARK MODEL

With new additive contributions to CP violating decay asymmetries, the asymmetries are no longer sines of SM unitarity triangle angles. However, they are still sines of the overall phases of the amplitudes in the asymmetries. We analyze the FDQM with the present data, and also show projected results for three different sin(2α) values of -1.0, 0, and $+1.0$, which are allowed under the FDQM, although sin(2α)=$\pm$1 are not allowed by the SM at 2σ.

A. sin(2β) and sin(2α)

In the four down quark model we use "sin(2α)" and "sin(2β)" to denote results of the appropriate B_d decay CP violating asymmetries, but since the mixing amplitudes are superpositions, the experimental results for these asymmetries are not directly related to angles in a triangle. Being imaginary parts of pure complex exponentials, they are sines of phase angles. The asymmetries with FCNC contributions included are (for $\bar{B}$ mixing to B before decay)

$$\sin(2\beta)\equiv A_{B_d^0\to\Psi K_s^0} = \mathrm{Im}\left[\frac{(U^2_{std-db}+U^2_{db})}{|U^2_{std-db}+U^2_{db}|}\frac{(V^*_{cb}V_{cs})}{(V_{cb}V^*_{cs})}\frac{(V^*_{us}V_{ud})}{(V_{us}V^*_{ud})}\right] \tag{11}$$

$$\sin(2\alpha)\equiv -A_{B_d^0\to\pi^+\pi^-} = -\mathrm{Im}\left[\frac{(U^2_{std-db}+U^2_{db})}{|U^2_{std-db}+U^2_{db}|}\frac{(V^*_{ub}V_{ud})}{(V_{ub}V^*_{ud})}\right] \tag{12}$$

with U^2_{std-db} defined in Eq. (9). The same mixing phase occurs in both asymmetries, times the squares of the different decay phases. We take the Moriond results for sin(2β) from Babar [13] and Belle [14,15] to give the weighted average sin(2β)=0.78$\pm$0.08.

B. sin(γ)

In the four down quark model, what we mean by "sin(γ)" is the result of the experiments which would give this variable in the SM [16,17], as in $B_s^0\to D_s^+K^-$. Here, the four down quark model involves more complicated amplitudes, and "sin(γ)" is not simply sin(δ_{13}):

$$\sin(\gamma)\equiv \mathrm{Im}\left[\frac{(U^2_{std-sb}+U^2_{sb})}{|U^2_{std-sb}+U^2_{sb}|}\frac{(V^*_{ub}V_{cs})}{|V^*_{ub}V_{cs}|}\frac{(V^*_{cb}V_{us})}{|V^*_{cb}V_{us}|}\right], \tag{13}$$

where

$$U^2_{std-sb}\equiv[\alpha/(4\pi\sin\theta_W^2)]y_t f_2(y_t)(V^*_{ts}V_{tb})^2. \tag{14}$$

In the SM, $U^2_{std-sb}=10\times10^{-6}$.

C. The "frequency" of B_s oscillations, x_s

In the four down quark model, x_s is no longer the simple ratio of two CKM matrix elements, but now involves the Z-mediated annihilations and exchange amplitudes as well. Here we avoid the full theoretical uncertainty on $B_B f_B^2$, by taking the ratio of x_s to x_d, which is better calculated theoretically, and in which we have also included the FCNC with Z^0 exchange

$$x_s=\frac{\Delta m_s}{\Gamma_{B_s}}=1.35x_d\frac{|U^2_{std-sb}+U^2_{sb}|}{|U^2_{std-db}+U^2_{db}|}. \tag{15}$$

We now include the amplitude method analysis of LEP with SLD to assign a $\Delta\chi^2$ for each Δm_s calculated in the angular parameter grid [18].

D. The B_s decay asymmetry, sin(2ϕ_s)

In the standard model, B_s mixing involves $(V^*_{ts}V_{tb})^2$ which is almost exactly real, and the leading decay process of $b\to c\bar{c}s$ has no significant phase from the decay which is proportional to V^2_{cb}. Thus almost no CP violating phase develops in the most likely B_s decays. This occurs in the decays $B_s\to J/\Psi\phi$, $B_s\to D_s^+D_s^-$, and $B_s\to J/\Psi K_S$. The near vanishing of this asymmetry is a test of the SM [6]. Below, we will find a strange twist on this, since the FDQM will include a range that includes values smaller than the SM range, and does not exceed it. In the SM the angle ϕ_s is the small angle in the b-s unitarity triangle, and its nonzero value indicates CP violation.

In the four down quark model, the CP violating B_s decay asymmetry is (for the mixing to $J/\psi\phi$ or $D_s^+D_s^-$ without the final K_S)

$$\sin(2\phi_s)=-\mathrm{Im}\left(\frac{(U^2_{std-sb}+U^2_{sb})}{|U^2_{std-sb}+U^2_{sb}|}\frac{(V^*_{cb}V_{cs})}{(V_{cb}V^*_{cs})}\right), \tag{16}$$

which includes the double FCNC Z^0 exchange proportional to U^2_{bs}. Because of the additional flavor changing term, in the four down quark model, the angle given by the above asymmetry will not generally be an angle in a triangle.

IV. FOUR DOWN QUARK MODEL AMPLITUDES IN KAON EXPERIMENTS

A. FCNC as an addition to penguin plus box amplitudes

Since CP violation and FCNC experiments with K mesons are approaching the SM range and also limit FCNC amplitudes, we now include the full SM amplitudes with the FCNC Z^0 exchange amplitudes as well. The K meson experiments are ϵ, $K^+\to\pi^+\nu\bar{\nu}$, $K_L\to\mu\mu$, and we now add the recent and fairly well determined results for Re(ϵ/ϵ').

We use the amplitudes determined by Buras [19,20]. In order to reconcile the notation between us and Buras and Silvestrini [21], we relate their Z_{ds} to our U_{sd} by taking

$$Z_{ds}=-\left(\frac{\pi^2}{\sqrt{2}G_F m_W^2}\right)U_{sd}, \tag{17}$$

as implied by their definitions in Lagrangians.

In the following formulas, B_0 is the $\Delta S=1$ box amplitude, S_0 is the $\Delta S=2$ box amplitude, C_0 is the Z^0 penguin amplitude, D_0 is the off-shell photon penguin (with D_0' being the on-shell amplitude), and E_0 is the off-shell gluon penguin (E_0' being on-shell). Gauge independent combinations are

$$X_0 = C_0 - 4B_0 \tag{18}$$

$$Y_0 = C_0 - B_0 \tag{19}$$

$$Z_0 = C_0 + \frac{1}{4}D_0. \tag{20}$$

For $m_t = 170$ GeV and $m_c = 1.25$ GeV, for example, these quantities are $S_0(x_t) = 2.46$, $S_0(x_c) = x_c$, $S_0(x_c, x_t) = 0.0022$, $X_0 = 1.57$, $Y_0 = 1.02$, $Z_0 = 0.71$, $E_0 = 0.26$, $D_0' = 0.38$, and $E_0' = 0.19$.

The FCNCZ^0 exchange with amplitude U_{ds} can be added to the d-s Penguin amplitude with the Z^0 by the substitution

$$\lambda_t C_0(x_t) \rightarrow \lambda_t C_0(x_t) - \frac{\pi^2}{\sqrt{2} G_F M_W^2} U_{sd}, \tag{21}$$

to obtain the SM plus FCNC result.

B. Indirect *CP* violation in epsilon

In K-$\bar{K}$ mixing, the small indirect CP violation is given through $|\epsilon|$ [19],

$$|\epsilon| = \frac{1}{\sqrt{2}\Delta M_K} |\mathrm{Im} M_{12}|, \tag{22}$$

where we include the substitution from Eq. (21):

$$M_{12} = \frac{G_F^2}{12\pi^2} F_K^2 \hat{B}_K m_{K^0} M_W^2 [\lambda_c^{*2} \eta_1 S_0(x_c) + \lambda_t^{*2} \eta_2 S_0(x_t) + 2\lambda_c^* \lambda_t^* \eta_3 S_0(x_c, x_t)] - \frac{\sqrt{2} G_F}{12} F_K^2 \hat{B}_K m_{K^0} U_{sd}^2. \tag{23}$$

The short distance QCD corrections factors in NLO are [19] $\eta_1 = 1.38 \pm 0.20$, $\eta_2 = 0.57 \pm 0.01$, and $\eta_3 = 0.47 \pm 0.04$, and we use $\hat{B}_K = 0.85 \pm 0.13$.

C. Direct *CP* violation in Re(ϵ'/ϵ)

The direct CP violation in K^0 decays, Re(ϵ'/ϵ), has received more accurate measurements that are definitely nonzero. The average of KTeV [22] and NA48 [23] gives Re(ϵ'/ϵ) = 17.3 ± 2.4, where the error has been increased by $\sqrt{(\chi^2/df)}$. The sum of the SM [19,20] plus FCNC amplitude from Eq. (21) is

$$\mathrm{Re}(\epsilon'/\epsilon) = \mathrm{Im}\,\lambda_t F_{\epsilon'} - \frac{\pi^2}{\sqrt{2} G_F M_W^2} \mathrm{Im}\, U_{sd}[P_X + P_Y + P_Z], \tag{24}$$

where

$$F_{\epsilon'} = P_0 + P_X X_0(x_t) + P_Y Y_0(x_t) + P_Z Z_0(x_t) + P_E E_0(x_t). \tag{25}$$

The P's are functions of $B_6^{1/2} = 1.0 \pm 0.3$, $B_8^{3/2} = 0.8 \pm 0.2$, and $\Lambda_{\overline{\mathrm{MS}}}^{(4)} = 340 \pm 50$ MeV [19].

D. $K^+ \rightarrow \pi^+ \nu \bar{\nu}$

The recent detection of two events in $K^+ \rightarrow \pi^+ \nu \bar{\nu}$ has produced the experimental result [24]

$$\mathrm{BR}_{\mathrm{expt}}(K^+ \rightarrow \pi^+ \nu \bar{\nu}) = (1.57^{+1.75}_{-0.82}) \times 10^{-10} \tag{26}$$

compared to the SM range [25] of $(0.72 \pm 0.21) \times 10^{-10}$. The Poisson probability for the angle parameters is converted to a chi-squared form [26] which is convolved into the total χ^2 formula. For this experiment using a logarithmic prior, with $2 \times n_{obs} = 4$ degrees of freedom [26], the addition to χ^2 is

$$\chi^2 = 2\langle n \rangle = 2 \times (2\ \text{events}) \times \frac{\mathrm{BR}_{\mathrm{calc}}}{\mathrm{BR}_{\mathrm{expt}}}. \tag{27}$$

The sum of the SM [19] plus FCNC contributions is obtained by using Eq. (21):

$$\begin{aligned}\mathrm{BR}_{\mathrm{calc}}(K^+ \rightarrow \pi^+ \nu \bar{\nu}) &= r_K \mathrm{BR}(K^+ \rightarrow \pi^0 e^+ \nu) \frac{\alpha^2}{|V_{us}|^2 2\pi^2 \sin^4 \theta_W} \\ &\times \left[2 \left| \lambda_c X_{NL}^e + \lambda_t X(x_t) - \frac{\pi^2}{\sqrt{2} G_F M_W^2} U_{sd} \right|^2 + \left| \lambda_c X_{NL}^\tau + \lambda_t X(x_t) - \frac{\pi^2}{\sqrt{2} G_F M_W^2} U_{sd} \right|^2 \right].\end{aligned} \tag{28}$$

Here, $X(x_t) = \eta_X X_0(x_t)$, etc., and [27] $\eta_X = 0.994$. Without the SM, the contribution of the Z^0 exchange alone with amplitude U_{sd} is $\chi^2 = 1.61 \times 10^9 |U_{sd}|^2$.

E. $K_L \rightarrow \mu^+ \mu^-$

The short distance weak FCNC contribution to $K_L \rightarrow \mu\mu$ constrains Re(U_{ds}) and is given from [28] after including Eq. (21):

$$\begin{aligned}\mathrm{BR}(K_L \rightarrow \mu^+ \mu^-) &= \mathrm{BR}(K^+ \rightarrow \mu^+ \nu) \frac{\tau_{K_L}}{\tau_{K^+}} \frac{\alpha^2}{|V_{us}|^2 \pi^2 \sin^4 \theta_W} \\ &\times \left(\mathrm{Re}\lambda_c Y_{NL} + \mathrm{Re}\lambda_t Y(x_t) - \frac{\pi^2}{\sqrt{2} G_F M_W^2} \mathrm{Re} U_{sd} \right)^2.\end{aligned} \tag{29}$$

Here, $Y(x_t) = \eta_Y Y_0$, and [27] $\eta_Y = 1.012$. The long distance contribution has been analyzed [29]. We make the 1σ limit conservatively as the sum of the 1σ experimental limit plus the 1σ long distance estimate [29].

From the above K meson formulas, the error formulas were generated using MATHEMATICA.

V. JOINT CHI-SQUARED ANALYSIS OF THE SM AND THE FDQM EXPERIMENTS

FCNC experiments put limits on the new mixing angles and constrain the possibility of new physics contributing to B_d^0-$\overline{B}_d^0$ and B_s^0-$\overline{B}_s^0$ mixing. Here we jointly analyze all constraints on the 4×4 mixing matrix obtained by assuming only one of the $\mathrm{SU}(2)_L$ singlet down quarks mixes appreciably [7]. We use the seven experiments for the 3×3 CKM submatrix elements [2], which include those on the three matrix elements V_{us}, V_{ub}, V_{cb} of the u and c quark rows; $|\epsilon|$; B_d-$\overline{B}_d$ mixing (x_d); the new limits on Δm_s, or x_s; and the new measurements for $\sin(2\beta)$. For studying FCNC, we include V_{ud} and V_{cd}, the bound on $B\to\mu\mu X_s$ (which constrains $b\to s$), the two events in $K^+\to\pi^+\nu\overline{\nu}$ [12,26,30], and R_b in $Z^0\to b\overline{b}$ [12] (which directly constrains the V_{4b} mixing element). FCNC experiments will bound the three amplitudes U_{ds}, U_{sb}, and U_{bd} which contain three new mixing angles and three phases. We use the mass of the top quark as $m_t=174$ GeV. We also add FCNC constraints from $K_L\to\mu\mu$, now including the large long distance error, and the new and more convergent results for ϵ'/ϵ from NA48 [23] and KTeV [22].

Related analyses including both SM and FDQM amplitudes in kaon constraints by Barenboim, Botella and Vives [31,32] precede this work. We have applied a full χ^2 analysis rather than just 95% C.L. bounds, and have included the new, larger and more exact $\sin(2\beta)$ results, as well as new $K^+\to\pi^+\nu\overline{\nu}$, ϵ'/ϵ results, and new and full x_s data. We have also included an analysis of the 4×4 mixing matrix parameters and found a crucial cancellation in one of the matrix elements.

We use a method for combining the Bayesian Poisson distribution for the average for the two observed events in $K^+\to\pi^+\nu\overline{\nu}$ [24,26] with the chi-squared distribution from the other experiments. This treats the two events with a logarithmic Bayesian prior as four degrees of freedom. This gives a total of ten additional experimental degrees of freedom for the FDQM.

In maximum likelihood correlation plots, we use for axes two output quantities which are dependent on the mixing matrix angles and phases, such as (ρ,η), and for each possible bin with given values for these, we search through the nine dimensional angular data set of the 4×4 down quark mixing angles and phases, finding all sets which give results in the bin, and then put into that bin the minimum χ^2 among them. To present the results, we then draw contours at several χ^2 in this two dimensional plot corresponding to given confidence levels.

A. Standard model $(\sin(2\alpha),\sin(2\beta))$ plot—present constraints

For the SM we take $\lambda=V_{us}$ as fixed and then use the six experiments on the 3×3 CKM matrix elements named above with three parameters to give three degrees of freedom. In the figures we show the χ^2 contours with confidence levels (C.L.) at values equivalent to 1σ, 90% C.L. (1.64σ), and 2σ. The new BaBar [33] and Belle [14,15] average is $\sin(2\beta)=0.78\pm0.08$. This gives $\beta=25.6°{}^{+4.0°}_{-7.4°}$. From Fig. 2 for the SM we see that the $\sin(2\beta)$ range is from 0.63 to 0.96 at 2σ, centered around the experimental average of 0.78. The SM $\sin(2\alpha)$ range at 2σ is from -0.90 to $+0.57$.

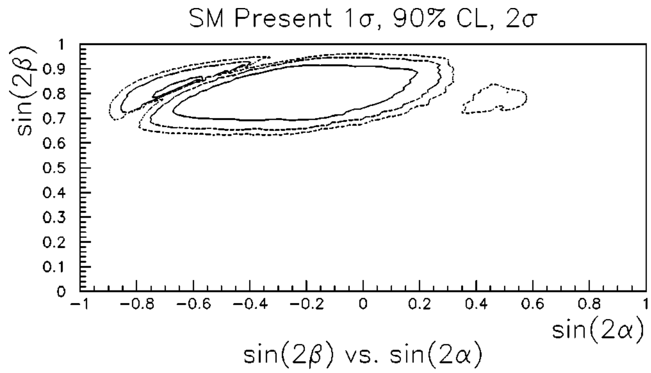

FIG. 2. The $(\sin(2\alpha),\sin(2\beta))$ plot for the standard model with contours at 1σ, 90% C.L., and 2σ with present data.

B. Four down quark model $(\sin(2\alpha),\sin(2\beta))$ plots—present limits

In the FDQM analysis including FCNC experiments, there are 17 experimental degrees of freedom, minus 9 parameters, giving 8 remaining degrees of freedom. In contrast to the SM, for the FDQM in Fig. 3, almost the entire region $\sin(2\beta)>0.48$ is allowed at 2σ, and $\sin(2\beta)$ can be as low as 0.55 at 1σ. In the FDQM, all values of $\sin(2\alpha)$ are allowed. In this case, the larger 1σ range for $\sin(2\beta)$ than from the direct experimental measurement is an effect of including so many experiments in the joint fit.

C. Standard model with comparison experiments (ρ,η) plot

Here we depart from the analysis of the SM experiments alone to show the effects of the additional three K meson experiments, namely $K^+\to\pi^+\nu\overline{\nu}$, $K_L\to\mu\mu$, and ϵ'/ϵ.

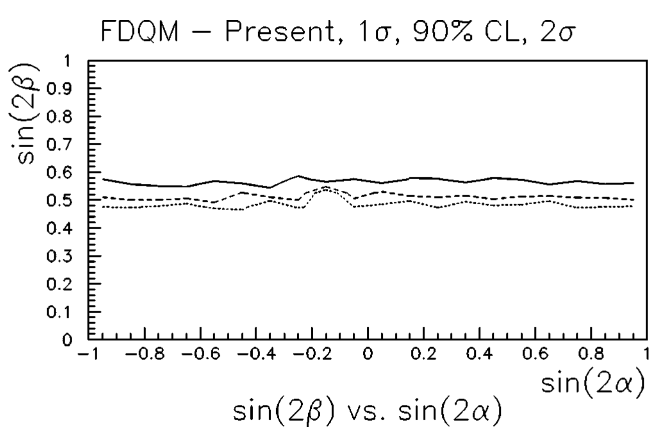

FIG. 3. The $(\sin(2\alpha),\sin(2\beta))$ plot for the FDQM with contours at 1σ, 90% C.L., and 2σ.

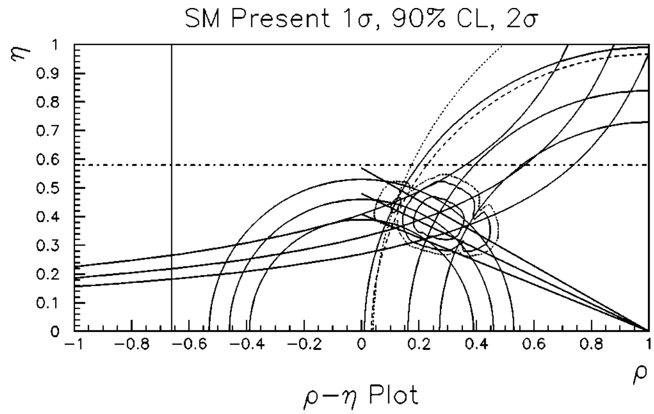

FIG. 4. The (ρ,η) plot for the SM with three comparison kaon experiments added, with joint χ^2 contours at 1σ, 90% C.L., and 2σ. The light lines are for the kaon experiments and are described in the text.

While they are not needed in the SM analysis, they are included in the FDQM analysis. In this case, there are 13 experimental degrees of freedom, minus 4 parameters, giving a net 9 degrees of freedom. Contours are at 1σ, 90% C.L., and 2σ. The three new K meson experimental contours for the SM are shown in Fig. 4. For ϵ'/ϵ, the lower 1σ contour is the horizontal dot-dashed line, where the central contour would be a horizontal line at $\eta=1.1$. For $K_L\rightarrow\mu\mu$ the solid vertical line at $\rho=-0.66$ is the lower 1σ contour with the central contour being a vertical line at $\rho=0.9$, which is not shown. This includes conservatively a large and uncertain long distance effect [29]. For $K^+\rightarrow\pi^+\nu\bar{\nu}$ the dotted contour giving an additional $\chi^2=1$ is the arc of the circle centered about $(\rho,\eta)=(1.3,0)$. It is not quite as restrictive in the SM as the 90% C.L. from the x_s or Δm_s limit, which is shown as the dotted quarter-circle about $(\rho,\eta)=(1.0,0)$. For the rest of the SM analysis we drop these three new K meson experiments.

D. Standard model: (ρ,η) plot

For the SM (ρ,η) plot in Fig. 5, the joint χ^2 enclosed

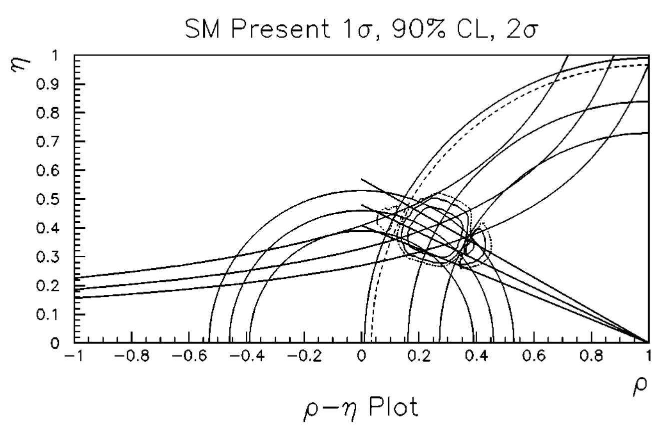

FIG. 5. The (ρ,η) plot for the standard model, showing the 1σ, 90% C.L., and 2σ contours of the joint fit, and the central and 1σ contours of the various constraints.

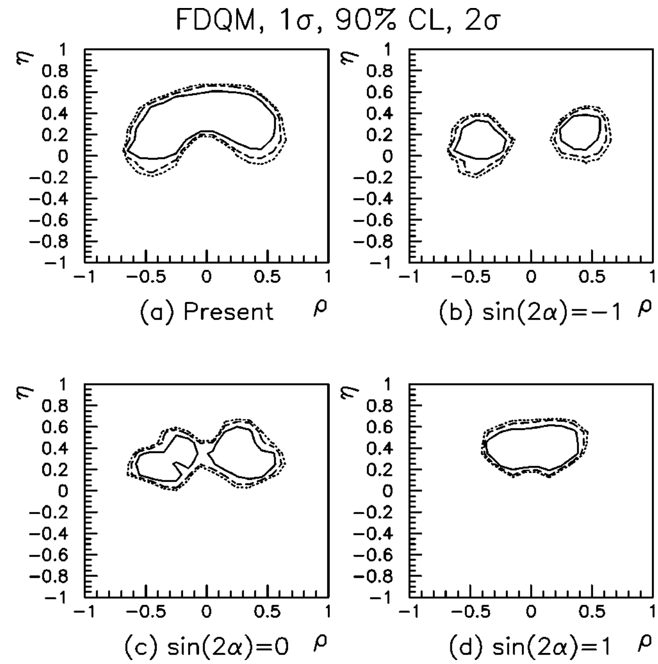

FIG. 6. The (ρ,η) plots for the four down quark model from: (a) present data, and for projected $\sin(2\alpha)$ values of -1, 0, and 1. Contours are at 1σ, 90% C.L., and 2σ.

contours are at 1σ, 90% C.L., and 2σ. The half-circles about $(\rho,\eta)=(0,0)$ are the center and 1σ contours for $|V^*_{ub}V_{ud}/V^*_{cb}V_{cd}|$. The hyperbolas are the center and 1σ contours for ϵ. The quarter circles about $(\rho,\eta)=(1,0)$ are for $|V_{td}|$ from x_d in B_d-$\bar{B}_d$ mixing. The lines emanating from $(\rho,\eta)=(1,0)$ are the central and 1σ limits for $\sin(2\beta)$. The Δm_s 90% circular arc is shown as the dashed quarter-circle, although the analysis weights each Δm_s or each V_{td} in χ^2. We see the effects of the $x_s=(\Delta m_s/\Gamma_s)=1.35x_d|V_{ts}/V_{td}|^2$ lower bound in the SM limiting the length of $V_{td}\propto\sqrt{(1-\rho)^2+\eta^2}$ and cutting off ρ for $\rho<0$.

E. Four down quark model: (ρ,η) plots

As in the SM, the plotted ρ and η are taken as the coordinates of V^*_{ub}, scaling the base of the b-d unitarity quadrangle to unity

$$\rho+i\,\eta\equiv V^*_{ub}V_{ud}/|V^*_{cb}V_{cd}|. \tag{30}$$

The unitaritity quadrangle is given by

$$V^*_{ub}V_{ud}+V^*_{cb}V_{cd}+V^*_{tb}V_{td}+V^*_{4b}V_{4d}=0 \tag{31}$$

where the last term has limits $|U_{bd}/V^*_{cb}V_{cd}|\leqslant 0.15$, as will be shown later. The near half circles in $\gamma=\delta=\delta_{13}$ ($V^*_{ub}=s_{13}e^{i\delta_{13}}$) at present are due to δ_{14} or δ_{24} (which are related) becoming some of the source of the observed CP violation in ϵ, so that δ_{13} is less constrained. Then, δ_{13} can be closer to zero or 180° so that η can also be small or zero. For projected $\sin(2\alpha)=+1$, 0, or -1, we see regions extended beyond the SM regions, which also allow η to be small (see Fig. 6). Examining the effect of each new K experiment

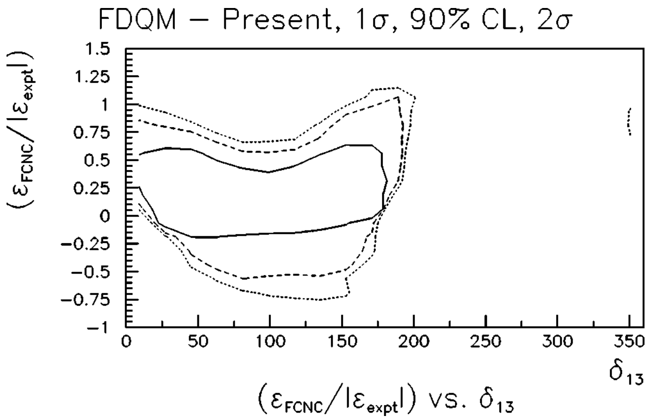

FIG. 7. The ratio ($\epsilon_{\mathrm{FCNC}}/|\epsilon_{\mathrm{expt}}|$) of the contribution of the FCNC amplitude to ϵ_K as a function of the angle δ_{13}.

separately, we find that the $K^+ \rightarrow \pi^+ \nu \bar{\nu}$ result eliminates the large 1σ negative η rings from the previous analysis [1].

F. Fraction of the new FCNC amplitude in ϵ

In order to display how the FCNC Z^0 exchange with the new phases in U_{ds} can account for the CP violation in ϵ_K, we plot the ratio of the FCNC contribution to the experimental result. In Fig. 7, ($\epsilon_{\mathrm{FCNC}}/|\epsilon_{\mathrm{expt}}|$) is shown against the phase of V_{ub}^*, which is δ_{13}. In Fig. 7, while ϵ_{FCNC} cannot account for the entire ϵ result, it can account for 60% of it at a 1σ confidence level.

G. Standard model: (x_s,sin(γ)) plots

x_s is determined in the SM from

$$x_s = 1.35 x_d (|V_{ts}|/|V_{td}|)^2. \qquad (32)$$

The largest error arises from the uncertainty in $|V_{td}|$, which follows from the present 15% uncertainty in $\sqrt{B_B} f_B = 230 \pm 35$ MeV from lattice calculations [34]. In the SM, the B factory measurements construct a rigid triangle from the knowledge of α and β, and removes this uncertainty in γ and x_s in the future.

From present data for the SM (x_s,sin(γ)) plot in Fig. 8, the limits at 2σ are $0.56 \leqslant \sin(\gamma) \leqslant 0.99$, and $16 \leqslant x_s \leqslant 48$. Because of the approximately linear relation between x_s and sin(γ), an exact x_s measurement ($\propto 1/|V_{td}|^2$) can strongly constrain sin(γ) to ± 0.07 in the SM.

H. Four down quark model: (x_s,sin(γ)) plots

In the FDQM, the sin(γ) range goes down to zero at 1σ, or -0.4 at 2σ (Fig. 9), since η now goes down to zero at 1σ or to -0.2 at 2σ where $\rho \approx -0.5$. A larger sin(γ) range is thus allowed in the FDQM than in the SM. The x_s allowed region in the FDQM is 16 to 60 at 1σ or to 80 at 2σ, which is also larger than the 2σ x_s range of 48 in the standard model. In the FDQM, there is not an approximately linear relation between sin(γ) and x_s as there is in the SM. Thus an accurate measurement of x_s still leaves a very large region of

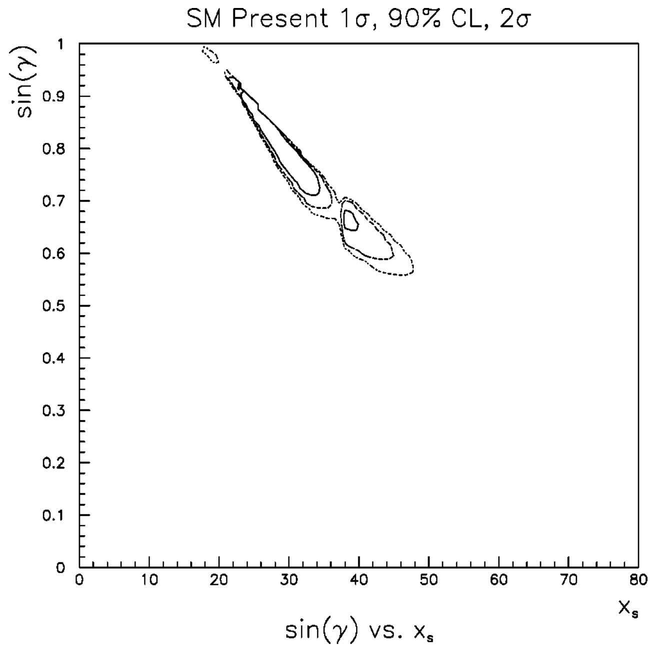

FIG. 8. The (x_s,sin γ) plot for the standard model with present limits with contours at 1σ, 90% C.L., and 2σ.

sin(γ) available in the FDQM. A subsequent sin(γ) measurement will be needed to distinguish between the two models.

I. The decay asymmetry from B_s mixing, sin($2\phi_s$)

ϕ_s is the small angle in the b-s unitarity triangle given by

$$V_{cb}^* V_{cs} + V_{tb}^* V_{ts} + V_{ub}^* V_{us} = 0. \qquad (33)$$

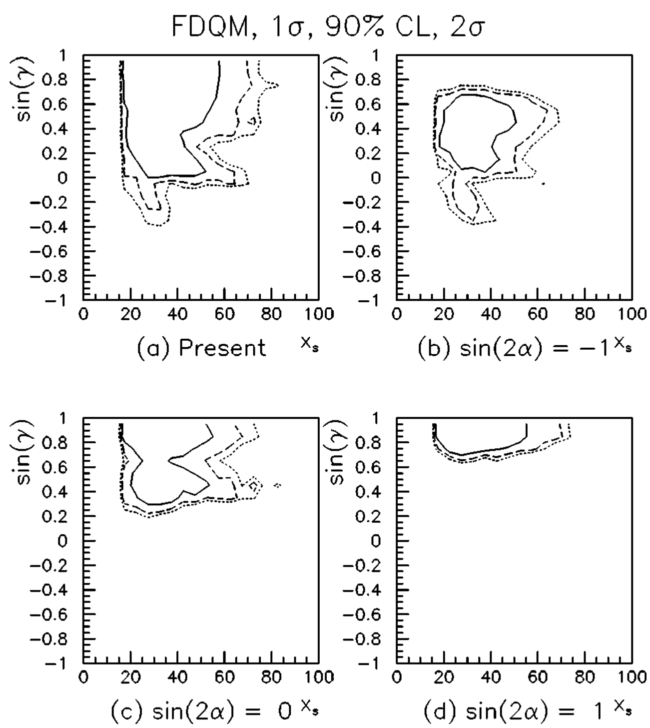

FIG. 9. The (x_s,sin(γ)) plots for the four down quark model from (a) present data, and (b), (c), and (d) for B factory cases for values of sin(2α) as labeled.

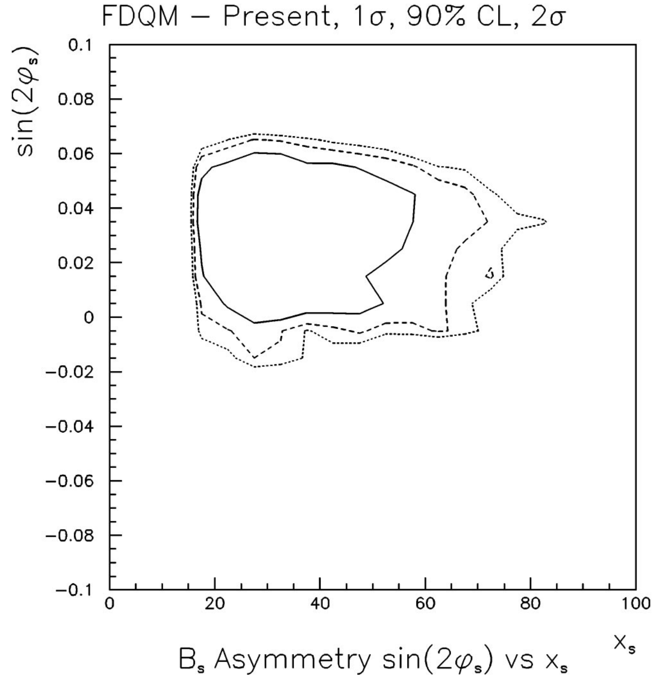

FIG. 10. The $(x_s, \sin(2\phi_s))$ plot for the B_s asymmetry $\sin(2\phi_s)$ in the four down quark model for present data, with contours at 1σ, 90% C.L., and 2σ.

In Wolfenstein terms this is

$$(A\lambda^2)\times 1+1\times[-A\lambda^2-A\lambda^4(\rho+i\eta)] +[A\lambda^3(\rho+i\eta)]\times\lambda=0. \tag{34}$$

Then, $\sin(\phi_s)=A\lambda^4\eta/A\lambda^2=\lambda^2\eta$. This is small in the standard model where $\sin(2\phi_s)=2\lambda^2\eta=0.10\eta$, or at 2σ

$$0.030\leqslant\sin(2\phi_s)\leqslant 0.060. \tag{35}$$

In the FDQM, as seen in Fig. 10, $-0.2\leqslant\sin(2\phi_s)\leqslant 0.065$ at 2σ, and down to zero at 1σ. Here the range continues down to zero since η can go down to zero. Hence, a value of $\sin(2\phi_s)$ less than 0. 03 would signify a deviation from the SM.

J. Fourth side of the unitarity quadrangle U_{bd}

Unitarity of the b-d columns has four terms, which may be written as

$$V_{ub}^*V_{ud}+V_{cb}^*V_{cd}+V_{tb}^*V_{td}-U_{bd}=0, \tag{36}$$

since $-U_{bd}=V_{4b}^*V_{4d}$. (We use $U_{db}=U_{bd}^*$.) As the unitarity triangle is scaled by $|V_{cb}^*V_{cd}|$ to make a unit base, the complex plot of U_{bd} is also so scaled. The length of the $U_{bd}/|V_{cb}^*V_{cd}|$ side, as plotted in Fig. 11, is thus less than 0.15, compared to the unit base in the (ρ,η) plot, and prefers possibly a more vertical direction. The accuracy of angles and sides of the unitarity triangle must and should reach this accuracy for a good test of the SM.

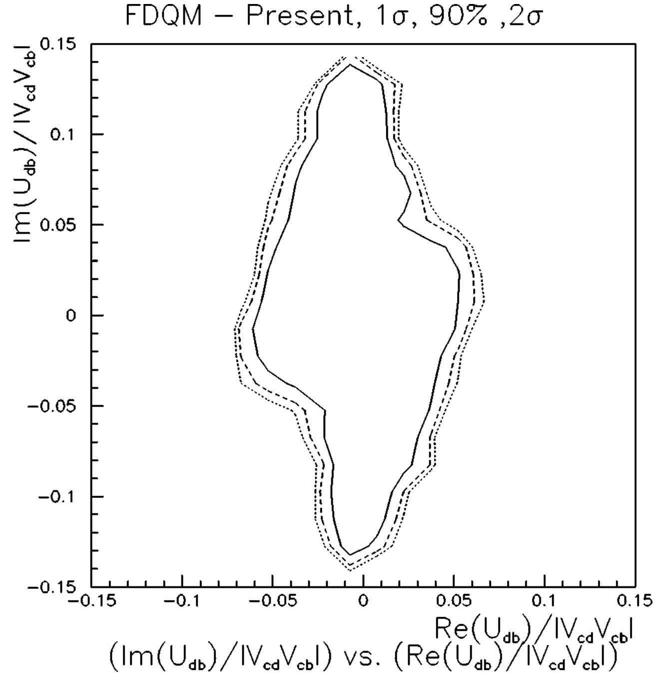

FIG. 11. The complex plot of U_{db} scaled to make it the fourth side of the unitarity quadrangle in the b-d unitarity plot.

VI. SIZE OF THE MIXING MATRIX ELEMENTS AND MIXING ANGLES

A. Bound from $Z^0\to b\bar{b}$

The weak isovector part of $Z^0\to b\bar{b}$ is reduced by $(1-|V_{4b}|^2)$ through

$$V^b=-\frac{1}{2}(1-|V_{4b}|^2)+\frac{2}{3}\sin^2\theta_W+\frac{1}{3}\rho_t,$$

$$A^b=-\frac{1}{2}(1-|V_{4b}|^2)+\frac{1}{3}\rho_t, \tag{37}$$

$$\Gamma^{std}(Z^0\to b\bar{b}) =\frac{C_{QCD}G_F m_Z^3}{6\sqrt{2}\pi}[(V^b)^2+(A^b)^2], \tag{38}$$

where $C_{QCD}=3(1.0385)$, and $\rho_t=0.0094$ for $m_t=174$ GeV. Present data and theory give

$$R_b^{\rm exp}=0.21642\pm 0.00073 \tag{39}$$

$$R_b^{\rm theory}=0.2158\pm 0.0003. \tag{40}$$

We note that the $|V_{4b}|$ effect is to decrease R_b, while the experiment is about 1σ above the theory. To lowest order in $|V_{4b}|$ the FDQM effect is

$$\frac{\Gamma_{b\bar{b}}^{std+FCNC}}{\Gamma_{b\bar{b}}^{std}}=(1-2.29|V_{4b}|^2). \tag{41}$$

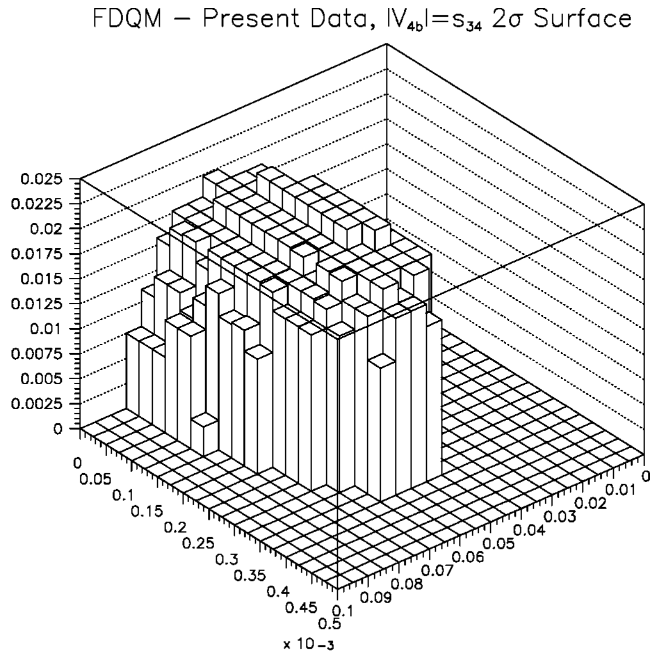

FIG. 12. The Lego plot for the height $|V_{4b}|\approx s_{34}$ at 2σ, on the base of $|V_{4s}|$ (units 10^{-3}) vs $|V_{4d}|\approx s_{14}$.

This gives a contribution to χ^2 of

$$\chi^2=(0.82+0.68\times 10^3|V_{4b}|^2)^2. \tag{42}$$

This χ^2 is used as a constraint on all angle choices in the fit. Taking the 90% C.L. limit at $\chi^2=(1.64)^2$ gives the bound on $|V_{4b}|$ from R_b alone of $|V_{4b}|\approx|s_{34}|\leqslant 0.035$.

B. 3D matrix element Lego plot

From the 2σ surface in the 3D space of the magnitudes of the matrix elements involved in the FCNC, Fig. 12, we can see the limits and ranges of two of the matrix elements. To 5% accuracy, $V_{4d}=-s_{14}e^{i\delta_{14}}$, and its magnitude ranges from 0.035 to 0.085 at 2σ. To 10% accuracy, $V_{4b}=-s_{34}$, and its magnitude ranges up to 0.020 at 2σ. The third FCNC matrix element, $|V_{4s}|$, is bounded by 0.0004. This requires a fine cancellation between its two components in $(-s_{24}e^{i\delta_{24}}-s_{12}s_{14}e^{i\delta_{14}})$, such that $s_{24}\approx s_{12}s_{14}$ and $\delta_{24}=\delta_{14}+\pi$ to get the cancelling minus sign. This means that there is effectively only one new phase, which we may consider as δ_{14}. From the cancellation, s_{24} ranges from 0.009 to 0.017 at 2σ. The cancellation is to about 1/20 of the value of s_{24}. The third term in V_{4s}, $s_{34}(s_{23}+s_{12}s_{13}e^{i\delta_{13}})$, then contributes $\leqslant 0.0009$, which is the same order as the partly canceling terms. The cancellation does not mean fine tuning since one could have parametrized V_{4s} by a single angle instead. However, the incredibly small size of $|V_{4s}|\leqslant\lambda^5$ could be considered a fine tuning itself. In comparison to the SM CKM matrix we should note that keeping the leading terms in the real and imaginary parts, $V_{cs}=1+iA^2\lambda^6\eta$, $V_{cd}=-\lambda-iA^2\lambda^5\eta$, and $V_{ts}=-A\lambda^2-iA\lambda^4\eta$. So even in the standard model there are matrix elements whose imaginary parts are as small as $O(\lambda^4)$, $O(\lambda^5)$, and $O(\lambda^6)$.

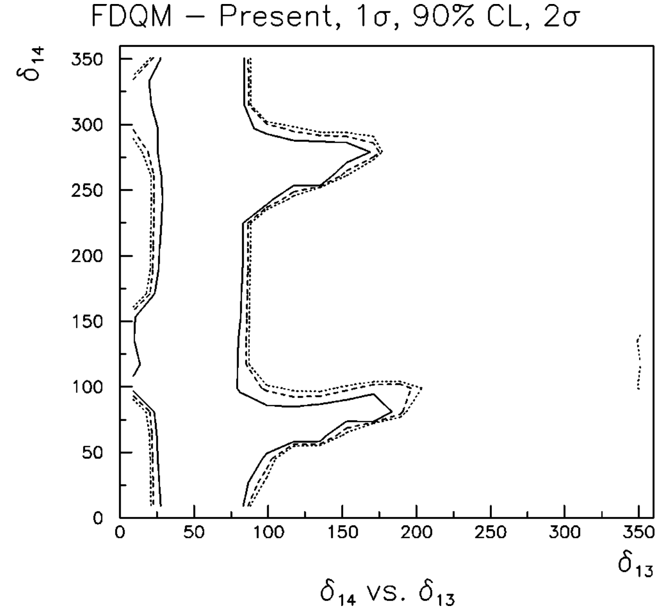

FIG. 13. Contour plot of δ_{14} vs δ_{13} with contours at 1σ, 90% C.L., and 2σ.

In Wolfenstein terms, $|V_{4d}|\approx s_{14}\approx\lambda^2$, $s_{24}\approx s_{12}s_{14}\approx\lambda^3$, $|V_{4b}|\approx s_{34}<\lambda^2/2$, but $|V_{4s}|\leqslant\lambda^5$. The sequence may violate the heirarchical expectation from the 3×3 CKM matrix.

In the double FCNC Z^0 exchange amplitude in B_d-$\overline{B}_d$ mixing, via

$$U_{db}=-V_{4d}^{*}V_{4b}\approx s_{14}e^{-i\delta_{14}}s_{34}, \tag{43}$$

it is only the δ_{14} phase in $(U_{db})^2\approx e^{-2i\delta_{14}}$ that can add to the SM box diagram term with its phase of $(V_{td}^{*})^2$.

C. Phases

The cancellation in V_{4s} to make it small requires $\delta_{24}\approx\delta_{14}+\pi$. Thus we can display the phases in a two dimensional plot of δ_{14} vs δ_{13}, as in Fig. 13. When δ_{13} is in its SM range of 40° $[\sin(\gamma)=0.64]$ to 70° $[\sin(\gamma)=0.94]$ the SM terms can be dominant and the small FCNC amplitudes allow each δ_{14} equally. For certain values of δ_{14}, near 80° and 270°, the new physics amplitudes can be dominant and δ_{13} can be large, leading to the enlarged (ρ,η) contours that can reach $\eta\approx 0$ and extend beyond to $\delta_{13}\leqslant 200°$ at 2σ.

D. FCNC phase structure

Using the V_{4s} cancellation structure with $s_{24}=s_{12}s_{14}$ and $\delta_{24}=\delta_{14}+\pi$, we can rewrite the V_{4i} matrix elements in terms of just one phase in the leading terms

$$V_{4d}\approx-s_{14}e^{i\delta_{24}}\approx s_{14}e^{i\delta_{14}} \tag{44}$$

$$V_{4b}\approx-s_{34} \tag{45}$$

$$V_{4s}\approx(s_{24}-s_{12}s_{14})e^{i\delta_{14}}+s_{34}s_{23}. \tag{46}$$

To leading order, it is clear that only the two new phases (of which only one is effectively independent) are included in the V_{4i}, and therefore in the U_{ij} and in the FCNC amplitudes. The SM phase δ_{13} does not appear in the leading terms of U_{ij}.

The FCNC couplings, using the cancellation relations, are

$$U_{ds}=-s_{14}[(s_{24}-s_{12}s_{14})+s_{34}s_{23}e^{-i\delta_{14}}], \tag{47}$$

$$U_{sb}=s_{34}[(s_{24}-s_{12}s_{14})e^{-i\delta_{14}}+s_{34}s_{23}], \tag{48}$$

$$U_{db}=s_{14}s_{34}e^{-i\delta_{14}}. \tag{49}$$

We note that while s_{14} and s_{24} are nonzero, the cancellation in V_{4s} and the ability of s_{34} to vanish still allow all U_{ij} to vanish.

E. Variable determination

In general for the three complex matrix elements V_{4i}, one would expect three magnitudes and three phases. In determining these from the $-U_{ij}=V_{4i}^*V_{4j}$ however, one overall phase would not appear experimentally, due to the V^*V structure of the U_{ij}. So we can at best determine three magnitudes and two phases from the U_{ij}. This agrees with the three new angles and two new phases introduced in the 4×4 unitary matrix where an extra phase has been removed for the definition of the new D^0 down quark. Whereas the three U_{ij} may seem to contain three real and imaginary parts to be determined, they are not independent, since there is one restriction between them, namely that the product

$$U_{ds}U_{sb}U_{bd}=|V_{4d}|^2|V_{4s}|^2|V_{4b}|^2 \tag{50}$$

is real. So again, we are left with three magnitudes and two phases that can be determined by experiments involving the FCNC amplitudes, which allows us to determine the three new angles and two new phases, just from low energy experiments involving the U_{ij}.

With sufficient energy to produce one D quark, the angles s_{i4} can each be determined separately by the combined weak production of $\overline{u}D$, $\overline{c}D$ or $\overline{t}D$ pairs, or from the similar decays of the D quarks.

The cancelation in V_{4s} has related $s_{24}=\lambda s_{14}$ and $\delta_{24}=\delta_{14}+\pi$. Thus there are only effectively two independent new angles and one new phase to be determined from the five independent components of the U_{ij}, leading to an overconstrained system. Finding a consistent solution is then a test of the FDQM. Of course, if more variables are found to be needed, the mixings to five or six down quarks would have to be considered. The present fits have found nonzero values for s_{14} and its related s_{24}. Yet s_{34} may still be small or vanish, and the one new independent phase is still to be determined, although its determination is coupled to that of the CKM δ_{13} phase.

F. Unitarity tests on the CKM submatrix

Contained in the 4×4 analysis are tests of the unitarity of the 3×3 CKM submatrix contained in the 4×4 FDQM mixing matrix. The FCNC couplings U_{ds}, U_{sb}, and U_{db} measure the deviations from orthogonality of the columns of the CKM submatrix, in d-s, s-b, and d-b projections, respectively. Their sizes will be discussed in Sec. VI G under unitarity quadrangles.

Bounds on the size of the $|V_{4i}|$, i=1, 2, 3, bound the deviation from unity of the sum of the squares of the three CKM elements in each column

$$1-(|V_{ui}|^2+|V_{ci}|^2+|V_{ti}|^2)=|V_{4i}|^2. \tag{51}$$

Similarly, for the rows, the $|s_{i4}|^2$ measure the deviation from unity for the sum of the squares of the CKM row elements.

For the d column or u row, since $|V_{4d}|\cong s_{14}\approx0.035$ to 0.085, unitarity of the CKM three elements of the d column or u row is off by

$$0.0012\leqslant|V_{4d}|^2\leqslant0.0072, \quad \text{or} \tag{52}$$

$$0.5\lambda^4\leqslant|V_{4d}|^2\leqslant3\lambda^4. \tag{53}$$

For the s column, since $|V_{4s}|\leqslant0.40\times10^{-3}$, the deviation from unitarity of the CKM submatrix is bounded by

$$|V_{4s}|^2\leqslant0.16\times10^{-6}=0.6\lambda^{10}. \tag{54}$$

For the b column or t row, since $|V_{4b}|\cong s_{34}\leqslant0.020$, the deviation from unitarity of the CKM submatrix is bounded by

$$|V_{4b}|^2\leqslant0.00040=0.17\lambda^4\approx\lambda^5. \tag{55}$$

For the c row, since $s_{24}\cong s_{12}s_{14}=\lambda s_{14}$, the deviation of the CKM from unitarity is a multiple of the u row result from s_{14}

$$0.5\lambda^6\leqslant|s_{24}|^2\leqslant3\lambda^6. \tag{56}$$

Finally, the deviation of $|V_{44}|^2$ from unity is an overall measure of mixing to the fourth down quark

$$1-|V_{44}|^2=s_{14}^2+s_{24}^2+s_{34}^2. \tag{57}$$

The right-hand side is dominated by s_{14}^2 giving

$$|V_{44}|^2=1-(0.5\rightarrow3)\lambda^4. \tag{58}$$

G. Unitarity quadrangle completion

1. b-d quadrange

The orthogonality relation between the b and d columns of the 4×4 mixing matrix is

$$V_{ub}^*V_{ud}+V_{cb}^*V_{cd}+V_{tb}^*V_{td}-U_{db}^*=0. \tag{59}$$

The fourth side of the b-d unitarity quadrangle, scaled to make the base of unit length, is $U_{db}^*/|V_{cd}^*V_{cb}|$. From Fig. 11, we see that the length of the FCNC quadrangle side is $\leqslant0.15$ in the vertical or imaginary direction, and $\leqslant0.06$ in the horizontal or real direction. The sides of the b-d unitarity quadrangle can be written in a modified Wolfenstein form as

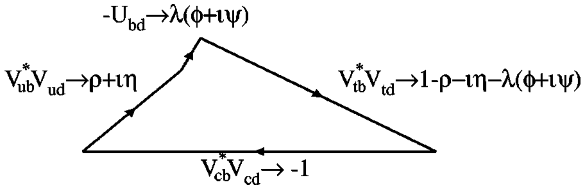

FIG. 14. The b-d unitarity quadrangle scaled by $A\lambda^3$, with sides given as above.

$$V^*_{ub}V_{ud}=A\lambda^3(\rho+i\eta), \tag{60}$$

$$V^*_{cb}V_{cd}=-A\lambda^3, \tag{61}$$

$$V^*_{4b}V_{4d}=-U^*_{db}=-s_{14}s_{34}e^{i\delta_{14}} \tag{62}$$

$$\equiv A\lambda^4(\phi+i\psi), \text{ and} \tag{63}$$

$$V^*_{tb}V_{td}=A\lambda^3[1-\rho-i\eta-\lambda(\phi+i\psi)], \tag{64}$$

where we have introduced $\phi+i\psi$ into $-U^*_{db}$ with a coefficient to make the scaled quadrangle A independent. An example of the scaled b-d quadrangle is shown in Fig. 14. We see that unitarity requires that the length of the FCNC coupling side $-U^*_{db}$ has to be cancelled by another triangle side to close the triangle, and that occurs in $V^*_{tb}V_{td}$ having an addition to the SM formula. The area of the b-d unitarity quadrangle is computed by adding the areas of three subtriangles and a rectangle

$$\text{Area}(b-d)=A^2\lambda^6[\eta+(1-\rho)\psi]/2. \tag{65}$$

We note that if either or both η and ψ are nonzero, CP is violated, and the quadrangle has a nonzero area, analogous to the SM unitarity triangle result. However, as we will see below, the area of the b-d quadrangle is different from those of the other unitarity quadrangles by the ψ term above.

2. *s-b quadrangle*

The unitarity orthogonality between the s and b columns for the s-b quadrangle is

$$V^*_{us}V_{ub}+V^*_{cs}V_{cb}+V^*_{ts}V_{tb}-U_{sb}=0. \tag{66}$$

The first term is $A\lambda^4(\rho-i\eta)$, the second term is $A\lambda^2$, and the third term is $-A\lambda^2$, to leading order. If we scale the base to unit length by dividing by $A\lambda^2$, then the first term side is of order 0. 02 in length. From Fig. 15, the fourth side of scaled U_{sb} is of order 0. 0001, or 0.5% of the small third side of the triangle. The enclosed angle is then the same as in the SM, $\phi_s=\lambda^2\eta$, and the triangle's or quadrangle's area is $A^2\lambda^6\eta/2$.

3. *d-s quadrangle*

The orthogonality relation between the d and s columns is

$$V^*_{ud}V_{us}+V^*_{cd}V_{cs}+V^*_{td}V_{ts}-U_{ds}=0. \tag{67}$$

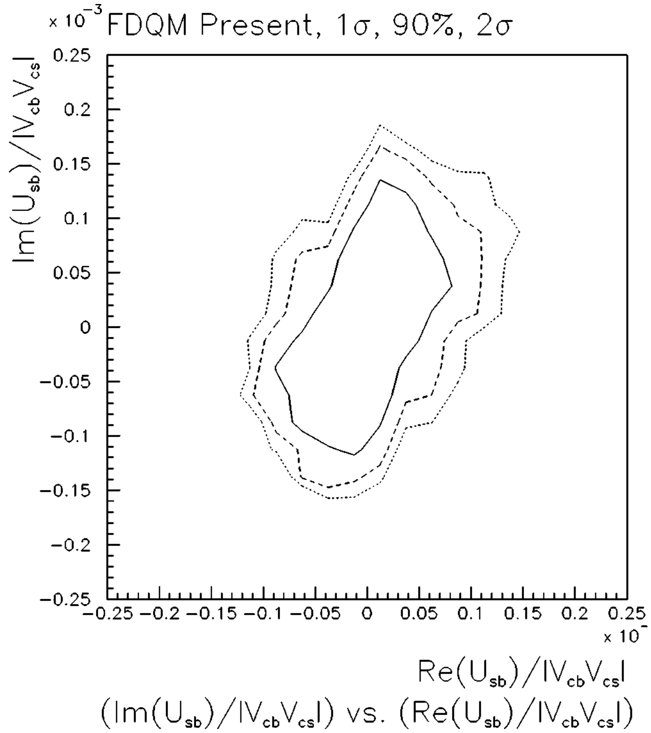

FIG. 15. Contours for the complex FCNC coupling U_{sb} scaled by $|V^*_{cs}V_{cb}|$, which is the fourth side of the s-b unitarity quadrangle.

The largest sides of the d-s unitarity quadrangle are of length λ, being the first and second terms, and the third term is $A^2\lambda^5(1-\rho+i\eta)=0.0004(1-\rho+i\eta)$. The fourth side is the FCNC coupling U_{sd}, which is bounded in magnitude by $2.5\times10^{-5}=\lambda^7$, as seen in Fig. 16. Thus the FCNC fourth

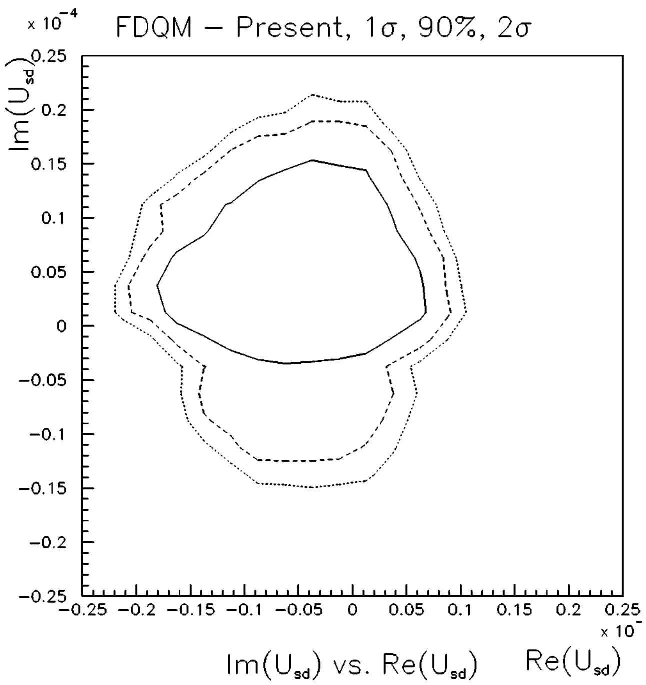

FIG. 16. Contours for the complex FCNC coupling U_{ds} which is the fourth side of the d-s unitarity quadrangle.

side is at most 6% of the small third side. The angle subtended by the small third side is then essentially the same as that by the third and fourth sides, being $\phi_d = A^2\lambda^4\eta$. The triangle's or quadrangle's area is also $A^2\lambda^6\eta/2$.

H. The sum rule for the *CP* violating *B* decay asymmetry angles

It was shown before [6] that as long as the penguin diagrams in the B decays can be neglected, that the sum of the CP violating decay angles, even with new physics contributions, is π modulo π. This can be seen from Eqs. (12) and (11) where in the sum of $(2\alpha+2\beta)$, the B_d mixing phase cancels out in general, regardless of its source, and from Eqs. (13) and (16), where in the sum of $(2\gamma+4\phi_s)$, the phase from B_s mixing cancels out. The other tree amplitude decay phases in these equations either cancel or sum to the phase of a product of mixing matrix elements which becomes a product of absolute values squared, with zero phase. This leads to the CP violating B decay angle sum rule [6]

$$\alpha+\beta+\gamma+2\phi_s=\pi, \quad \mathrm{mod}\ \pi. \tag{68}$$

VII. CONCLUSIONS FOR ISOSINGLET DOWN QUARK MODELS

With much new data, it is still the case that FCNCs can contribute significantly to B_d-$\overline{B_d}$ mixing and to B_s-$\overline{B_s}$ mixing, and give contributions with new phases. In the FDQM, all $\sin(2\alpha)$ are allowed. In the (ρ,η) plane, the FDQM allows large regions for $\rho\leqslant 0$ as opposed to the $\rho\geqslant 0$ regions in the SM, and in particular, those where η goes to zero, both with the present data and with the projected $\sin(2\alpha)$ values. In new physics models then, the SM phase δ, or η, can be smaller, with the other phases causing much of the presently observed CP violation. In the $(x_s,\sin(\gamma))$ plots in the FDQM, all of $\sin(\gamma)\geqslant 0$ is allowed at present in contrast to $\sin(\gamma)\geqslant 0.55$ in the SM, and with no approximately linear relation as in the SM. This will require combining experimental results of x_s and $\sin(\gamma)$, to find out if the results correlate to the narrow linear region of the SM analysis. The present range for x_s is from 16 to 48 at 2-σ in the SM, and from 16 to 80 at 2-σ in the four down quark model. The b-d unitarity triangle, scaled to unit base length, has to be measured to an accuracy of 0.15 or better to begin to limit a fourth side and to verify the SM against the FDQM.

Each E_6 generation also contains an isosinglet [4] or sterile neutrino, which may provide a connection between the quark and lepton searches for new physics in terms of establishing new particle representations.

The mass of the lightest singlet down quark in E_6 could be roughly related to the mixing angle by

$$\theta_{34}^2 \simeq m_b/m_D, \quad \text{and with} \quad |V_{4b}|\simeq\theta_{34}\leqslant 0.02 \tag{69}$$

from combined fits, that gives

$$m_D \geqslant 2500\times m_b = 11\ \ \mathrm{TeV}. \tag{70}$$

Using the single R_b 90% C.L. limit of $|\theta_{34}|\leqslant 0.035$, which is not as strong as the combined fits, gives $m_D\geqslant 4$ TeV. The previous analysis [1] gave a lower limit of 1.2 TeV.

ACKNOWLEDGMENTS

This research was supported in part by the U. S. Department of Energy under Contract No. DE-FG0391ER40679. We acknowledge the hospitality of SLAC. We thank Herng Tony Yao, Sheldon Stone, and David Kirkby for discussions.

[1] D. Silverman, Phys. Rev. D **58**, 095006 (1998).
[2] W.-S. Choong and D. Silverman, Phys. Rev. D **49**, 2322 (1994).
[3] D. Silverman, Int. J. Mod. Phys. A **11**, 2253 (1996).
[4] J.L. Hewett and T.G. Rizzo, Phys. Rep. **183**, 193 (1989).
[5] M. Shin, M. Bander, and D. Silverman, Phys. Lett. B **219**, 381 (1989).
[6] Y. Nir and D.J. Silverman, Nucl. Phys. **B345**, 301 (1990).
[7] Y. Nir and D.J. Silverman, Phys. Rev. D **42**, 1477 (1990).
[8] D. Silverman, Phys. Rev. D **45**, 1800 (1992).
[9] W.-S. Choong and D. Silverman, Phys. Rev. D **49**, 1649 (1994).
[10] F.J. Botella and L.-L. Chau, Phys. Lett. **168B**, 97 (1986).
[11] G.C. Branco, T. Morozumi, P.A. Parada, and M.N. Rebelo, Phys. Rev. D **48**, 1167 (1993).
[12] L. Lavoura and J.P. Silva, Phys. Rev. D **47**, 1117 (1993).
[13] BABAR Collaboration, B. Aubert *et al.*, hep-ex/0203007.
[14] Belle Collaboration, K. Abe *et al.*, Phys. Rev. Lett. **87**, 091802 (2001).
[15] Belle Collaboration, K. Trabelsi, in *XXXVII Recontres de Moriond* (2002), http://belle.kek.jp/bdocs/moriond02_karim.pdf
[16] R. Aleksan, I. Dunietz, and B. Kayser, Z. Phys. C **54**, 653 (1992).
[17] R. Aleksan, I. Dunietz, B. Kayser, and F. Le Diberder, Nucl. Phys. **B361**, 141 (1991).
[18] LEP B Oscillation Group, Results for La Thuile and Recontres de Moriond, Winter 2002, http://lepbosc.web.cern /LEPBOSC/combined_results/lathuile_2002/
[19] A.J. Buras, hep-ph/9905437.
[20] A.J. Buras, hep-ph/9806471.
[21] A.J. Buras and L. Silvestrini, Nucl. Phys. **B546**, 299 (1999).
[22] KTeV Collaboration, T. Yamanaka, Acta Phys. Pol. B **32**, 2171 (2001).
[23] NA48 Collaboration, B. Vallage, Acta Phys. Pol. B **32**, 1953 (2001).
[24] E787 Collaboration, S. Adler *et al.*, Phys. Rev. Lett. **88**, 041803 (2002).
[25] G. D'Ambrosio and G. Isidori, Phys. Lett. B **530**, 108 (2002).
[26] D. Silverman, physics/9808004.
[27] G. Buchalla and A.J. Buras, Nucl. Phys. **B548**, 309 (1999).
[28] A.J. Buras and R. Fleischer, hep-ph/9704376.
[29] G. D'Ambrosio, G. Isidori, and J. Portoles, Phys. Lett. B **423**, 385 (1998).

[30] E787 Collaboration, S.C. Adler *et al.*, Phys. Rev. Lett. **84**, 3768 (2000).
[31] G. Barenboim, F.J. Botella, and O. Vives, Phys. Rev. D **64**, 015007 (2001).
[32] G. Barenboim, F.J. Botella, and O. Vives, Nucl. Phys. **B613**, 285 (2001).
[33] BaBar Collaboration, B. Aubert *et al.*, Phys. Rev. Lett. **87**, 091801 (2001).
[34] C.W. Bernard, Nucl. Phys. B (Proc. Suppl.) **94**, 159 (2001).